Available online at www.sciencedirect.com

ScienceDirect

journal homepage: www.elsevier.com/locate/he

Dry reforming of methane over Co-Ce-M/AC-N catalyst: Effect of promoters (Ca and Mg) and preparation method on catalytic activity and stability

Yinghui Sun, Guojie Zhang, Ying Xu, Riguang Zhang*

Key Laboratory of Coal Science and Technology, Ministry of Education and Shanxi Province, Taiyuan University of Technology, Taiyuan, 030024, PR China

HIGHLIGHTS

- Mg or Ca modified 1Co-1Ce/AC-N catalysts were prepared for DRM reaction.
- The 1Co-1Ce-1Ca/AC-N catalyst exhibits excellent activity in DRM reaction.
- Improvement in catalytic performance is caused by higher active metal dispersion.
- The Co^{2+}/Co^{3+} and Ce^{3+}/Ce^{4+} as important species to promote electron transfer.

GRAPHICAL ABSTRACT

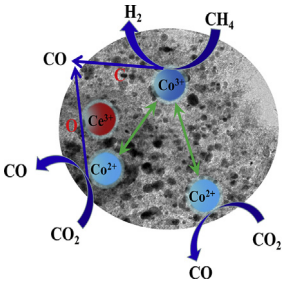

ARTICLE INFO

Article history:
Received 3 May 2019
Received in revised form
26 June 2019
Accepted 1 July 2019
Available online 20 July 2019

Keywords:
Bimetals Co-Ce
Dry reforming
N-doped activated carbon
Promoter
Calcium

ABSTRACT

The catalytic activity of DRM reaction over 1M-1Co-1Ce/AC-N (M = Ca and Mg) catalysts was investigated at 800 °C and under atmospheric pressure. By promoting N-doped activated carbon supported Co-Ce catalysts with alkaline-earth metals to obtain catalysts with better catalytic performance is the main purpose of study. The catalysts were prepared by wet-impregnation method and the influence of impregnation sequence on catalytic performance was also studied. The characterization was conducted using TPR, TPD, XPS, TEM and Raman. The catalyst 1Ca-1Co-1Ce/AC-N promoted with Ca and prepared by co-impregnation exhibited higher catalytic activity than unmodified. This was mainly due to the stronger interaction between metal and support as well as better active metals dispersion. The 1Ca-1Co-1Ce/AC-N catalysts also displayed excellent stability and XPS results indicated that higher Ce^{3+}/Ce^{4+} and $O_\beta/(O_\alpha+O_\beta)$ ratios were observed on this catalyst. However, the catalyst 1Co-1Ce/1Ca/AC-N prepared with sequential impregnation

* *Corresponding author.*
E-mail addresses: zhangguojie@tyut.edu.cn, zhgjdoc@126.com (G. Zhang).
https://doi.org/10.1016/j.ijhydene.2019.07.010

exhibited poor stability. In addition, the TEM of the spent catalysts revealed that there were a large number of carbons were generated on active metal surface.

Introduction

The emission of greenhouse gas (GHG) causes dramatic influence on global warming, especially for CO_2, its concentration in the ambient air has reached 400 ppm [1,2]. The dry reforming of CH_4 with CO_2 to syngas can not only take advantage of two of the biggest greenhouses, but also the appropriate CO/H_2 ratio can be directly used as raw gas for Fischer-Tropsch synthesis [3]. However, due to the high degree of carbon deposition and active metals sintering, the industrial application of DRM reaction has been limited [4–6]. Moreover, the DRM reaction is exothermic, which is also operated at relatively high temperature. Consequently, at present the research is mainly focused on preparing a highly efficient and stable catalyst.

Recently, DRM reaction has been widely studied over numerous supported catalysts such as Ni-based and Co-based catalysts [7,8]. Both metals are well-known for their use as a catalyst in many catalytic reactions including F-T synthesis [9], methane partial oxidation [10], ethanol steam reforming [11–13] and steam reforming of acetic acid [14]. In recent times, numerous studies have focused on Ni-based catalyst due to its high catalytic activity for DRM reaction. However, this kind of active metal is more prone to the generation of carbon deposition as well as metal sintering, and thus lead to catalyst deactivation. Due to its better anti-coking ability and low cost, Co-based catalysts also have been widely studied for DRM reaction, but the catalytic performance is relatively poor than Ni-based catalysts.

It is well known that support can also influence the performance of catalyst [15,16]. Carbon materials supported catalysts have been extensively investigated for DRM reaction, due to the exceptional thermal stability and large surface area [17–19]. Activated carbon is widely used as support for its higher specific surface area and stability as well as low cost in catalytic reaction [20–22]. Its high stability and specific surface area could greatly improve the dispersibility and stability of active metals. However, a certain amount of acid sites on activated carbon makes Co-based catalyst prone to reduce the adsorption and activation of CO_2, causing a poor catalytic performance. Therefore, the introduction of basic groups or alkaline metals to activated carbon is considered to be one of effective measure to compensate the negative influence of acid sites on Co-based catalyst and to furthermore accelerate the adsorption and activation of reactant.

It is apparent that there are various approaches could be conducted to develop catalyst with better catalytic performance for DRM reaction, such as improving chemical properties of support [23,24], designing multi-metal catalyst [25–27], using proper promoters [28–30].

By doping heteroatom on activated carbon to tailor the electronic structure around carbon atoms and enhance the adsorption of active sites, which could also improve the catalytic performance of carbon materials [31,32]. Because of its higher electronegativity than that of C, the nitrogen atom is one of the most used atoms in the catalytic reaction of carbon material. The introduction of nitrogen atoms not only can increase the positive charge density of adjacent carbon atoms, but also accelerate the transport rate of oxygen and catalytic reaction rate [33–35].

Due to the ability of periodic oxidation-reduction between 3 + and 4+, ceria could be used as a medium for storing oxygen in ORR reaction [36–38]. Co-Ce bimetallic catalysts prepared with different methods have been investigated to exhibit excellent catalytic performance for many reforming reactions, such as ethanol steam reforming [39], propane steam reforming [40], and dry reforming [41,42] reactions. Eddie et al. [39] prepared a series of $Co/CeO_2/YSZ$ bimetallic catalysts by vapor deposition method for ethanol steam reforming, the characteristic results showed that the combination of both Co^0 and Co^{2+} improved the adsorption of ethoxide groups and accelerated the formation of intermediate product in the reaction process. Jeong et al. [40] compared the catalytic performance of Co_xCe_y/Al_2O_3 catalysts with different Co/Ce ratio for the propane steam reforming reaction. The experiment results demonstrated that the addition of Ce not only increases the concentration of oxygen vacancies, but also improves the migration ability of oxygen. It is also advantageous to the generation of CO_2 and elimination of carbon deposition. A. Ipek et al. [41] prepared $Co\text{-}Ce/ZrO_2$ catalysts and found that the addition of Ce reduced the oxidation of Co during DRM reaction which lead to higher stability. There is no significant metal sintering and carbon formation on the spent catalysts surface, the excellent surface oxygen storage/transfer performance of Ce accelerated periodic redox of catalysts.

Alkali metals or alkaline-earth metals are the most extensively studied promoters for Co-based catalysts with different supports, such as carbon materials [43,44], SBA-15 [45] and SiO_2 [46] for catalytic reactions. Because the dispersion of active metals, the interaction between support and metals as well as the anti-coking performance of active metals are improving by adding promoters [47,48]. It is well known that adding a certain number of promoters on Co-based catalyst could also increase the catalytic performance for DRM reaction. Various alkaline-earth metals and alkaline oxides such as Ca [49], Mg [50], Na [51] and K [52] have been widely used as promoters for DRM reaction catalysts. Not only the great improvement of catalytic performance achieved by adding these promoters, but also they can be used on a large scale due to its low cost and easily accessible. It is generally supposed that the modified catalysts with these metals would enhance the interaction between metals and supports as well

as metal dispersion. The recent researches [53,54] have indicated that alkaline metals such as CaO, MgO and ZrO_2 could effectively restrain side reactions, since the addition of alkaline could improve the adsorption of CO_2, thus enhancing the content of basic sites of the support. The high concentration of CO_2 on catalyst surface is conducive to shift the equilibrium of Boudouard reaction to the left, thus, decreasing the generation of carbon deposition. A. Casanovas et al. [55] has studied the different promoters modified Co-based catalysts for steam reforming reaction. Compared with other promoters, Na modified Co/ZnO catalysts exhibited a higher catalytic performance and selectivity than unmodified catalysts. Jang et al. [56] has investigated the different alkaline earth metal oxides (CaO and MgO) as promoters modified Ni-based catalysts, the results showed that MgO modified catalyst displayed higher stability and deposition of carbon was successfully prevented at a very high reaction space velocity. The higher resistance to carbon deposition is due to strong Lewis basicity on Mg modified catalyst, causing excellent chemical adsorption of CO_2. The higher concentration of CO_2 is favour to eliminate the carbon deposition through CO disproportionation ($C+CO_2 = 2CO$). It reported that the MgO modified Co/Al_2O_3 showed better carbon deposition resistance than unmodified, thus the modified catalyst exhibited better stability and hydrogen selectivity [57]. This can be attributed to the basic feature of MgO, which increases the content of basic sites and accelerate the reaction of CO_2 and carbon deposition.

In this work, we used N-doped activated carbon as supports for the preparing of Co-Ce bimetallic catalyst via impregnation method, then different alkaline-earth metals Ca, Mg were used as promoters to modify Co-Ce catalysts. For one hand, the N-doped activated carbon is not only a convenient source of catalysts, but also the abundant functional groups which are beneficial to the redox reaction. The addition of Ca significantly improved the content of basic sites and enhanced the adsorption ability of CO_2. The Ca modified catalysts exhibited better anti-coking and higher catalytic performance compared with unmodified catalysts. The influence of the impregnation sequence of active metals and promoters was also examined. The sequence of impregnation the metals had significantly influence on the catalytic performance and stability.

Experiment

Material

Activated carbon (AC) was purchased from a local activated carbon factory. Melamine and all nitrates including cobalt nitrate ($Co(NO_3)_2\cdot 6H_2O$), cerium nitrate ($Ce(NO_3)_3\cdot 6H_2O$), magnesium nitrate ($Mg(NO_3)_2\cdot 6H_2O$) and calcium nitrate ($Ca(NO_3)_2\cdot 4H_2O$) were obtained from Aladdin Chemical Agent Company.

Preparation of N-doped activated carbon

Melamine (13.3 g) was dissolved into 80 v/v% ethanol aqueous solution (70 mL). The mixture was heated to 60 °C and 20 g of activated carbon was added into mixed solution. The mixture was stirred for 5 h at 60 °C followed by keeping it for 24 h at 105 °C. Then the samples were calcined at 650 °C for 2 h at nitrogen condition with a heating rate of 5 °C/min and the N-doped activated carbon (AC-N) was obtained.

Preparation of Mg/Ca modified Co-Ce catalyst

10 g $Co(NO_3)_2\cdot 6H_2O$, 14.92 g $Ce(NO_3)_3\cdot 6H_2O$ and 8.12 g $Ca(NO_3)_2\cdot 4H_2O$ or 8.81 g $Mg(NO_3)_2\cdot 6H_2O$ were dissolved in 70 mL distilled water. Then, 20 g AC-N was added in solution with vigorously stirring for 5 h at 25 °C. Then the mixtures were filtered and dried at 105 °C overnight. The samples were further calcined at 550 °C for 2 h. The catalysts made by co-impregnation method were donated as 1Co-1Ce-1Mg/AC-N or 1Co-1Ce-1Ca/AC-N. To further study the effect of impregnation sequence on catalytic performance. The impregnation sequence of active metals and promoters was adjusted during the preparation process. The impregnation order of Co-Ce and then Ca was denoted as 1Co-1Ce/1Ca/AC-N, another samples, preparing by the impregnation order of Ca and then Co-Ce was denoted as 1Ca/1Co-1Ce/AC-N.

Catalyst characterization

H_2-TPR profiles were obtained by Micromeritics AutoChem 2920 instrument, the powdery samples were loaded into quartz packed reactor. The TCD detector was used to record the consumption of H_2. The catalysts were outgassed at 300 °C for 30 min in an inert atmosphere and come to 30 °C. Then the samples were heated up to 900 °C with a 10 °C/min heating ramp under a reducing stream of 30 mL/min (10% H_2—Ar).

CO_2-TPD analysis was also carried out on Micromeritics AutoChem 2920. The sample was outgassed at 200 °C for 60 min under Ar atmosphere to dislodge some basic species from catalyst surface. Then the adsorption of carbon dioxide was carried at 50 °C under the mixture of CO_2/Ar gas (10% CO_2-Ar) with the total stream of 30 mL/min. Then heat the catalysts from 50 °C to 800 °C with the heating rate of 10 °C/min and the CO_2 signal was recorded by TCD detector.

XPS was conducted on a Thermo Scifentific Escalab 250Xi spectrometer. All catalysts were conducted in ultra-high vacuum by using Al-Kα X-ray source. For all Co and Ce binding energies were corrected with the graphitic C 1s signal at 284.8 eV. XPS peak 41 processing software was use for the peak deconvolution.

Morphologies of the calcined and spent catalysts were analyzed by TEM apparatus (JEM-2100, Jeol). Before the test can be performed, all catalysts were well dispersed over copper grids using ethanol, and the grids were dried at 80 °C for 24 h. Raman spectra were measured by the Renishaw spectrometer with the laser excitation at 514 nm and a grating of 2400 lines.

Catalytic test

The catalytic performance of DRM reaction was performed in a fixed bed reactor under atmospheric pressure, which contained a 25-mm-diameter quartz tube. 10 g of sample was loaded over the bed at the center of the reactor length. The fixed bed reactor was increased to 800 °C from room

temperature at N_2 flow of 80 mL/min at a rate of 10 °C/min. When the temperature reached 800 °C, the feed gas (120 mL/min, $CH_4/CO_2 = 1:1$) was introduced into the reactor. The flow rate of products after reaction was measured by soap-membrane flowmeter and the composition of products was determined by an online gas chromatograph (GC 950) which contained two carbon molecular sieve columns and two thermal conductivity detectors (TCD). The formulas below were used to calculate the CH_4 and CO_2 conversions:

$$X_{CH_4} = (1 - \frac{F_{out} \cdot C_{CH_4,out}}{F_{in} \cdot C_{CH_4,in}}) \times 100\%$$

$$X_{CO_2} = (1 - \frac{F_{out} \cdot C_{CO_2,out}}{F_{in} \cdot C_{CO_2,in}}) \times 100\%$$

where F and C represent the volume flow rate and the concentration of different gas composition, respectively.

Results and discussion

The interaction between metals and supports or metals as well as the reduction degree of catalysts were studied by H_2-TPR experiments. Fig. 1 displays the H_2-TPR profiles of catalysts, which were prepared with different promoters and impregnation sequence. The results indicated that the addition of different alkaline-earth metals had not significantly influence on the profile of reduction of the Co_3O_4 to Co^0. The profiles of all catalysts could be separated into two major reduction regions: an area that contains one peak around 300 °C and a higher temperature region, which comprises several peaks above 350 °C [58]. The first small reduction peak around 300 °C is designated to the reduction Co^{3+} to Co^{2+} which are easily reduced to Co^0, this because the interaction between metals and support are too weak, this reduction peak can also be attributed to bulk metal oxides [59]. The peak observed around 450 °C was attributed to the reduction of CoO to Co. Obviously, the reduction peaks at higher temperature can be assigned to the barely reducible Co-Ce bimetallic oxides. Compared with unpromoted catalyst, the reduce peaks shifted to higher temperature for catalyst, which promoted by Ca and prepared with co-impregnation method. In addition, comparing this profile with that of Mg promoted catalysts, it demonstrated that the addition of Ca increased the interaction between cobalt metal oxides and activated carbon. The peak area between 350 and 650 °C for 1Ca/1Co-1Ce/AC-N was significantly bigger than the other two Ca promoted catalysts, which prepared by different impregnation sequences. This could be related that the co-impregnation preparation method promoted the generation of Co-Ce bimetallic oxides.

CO_2-TPD experiments was used to examine the basicity of different calcined samples and the results have displayed in Fig. 2. Obviously, there are several peaks in the profiles of all catalysts. The peak around 150 °C can be assigned to the weak basic sites of catalysts. Obviously, the addition of promoters has significantly increased the content of weak basic sites. However, the intensity of this peak is almost same for the catalysts promoted by different alkaline earth metals and prepared by methods. The peak at about 450 °C was attributed to the medium strength basic sites. As for unpromoted catalyst, the intensity of this profile was much stronger, which mainly due to the hydroxyl group on the surface of the carbon material [60]. As for the desorption peaks around 550–850 °C, with the addition of Mg and Ca, the adsorption peaks of CO_2 became stronger and the temperature also changed, especially for 1Co-1Ce-1Ca/AC-N. The results indicated that the chemisorption of the CO_2 had been significantly improved the surface basic sites. It is generally acknowledged that basic sites on the catalyst surface can promote the adsorption and the dissociation of CO_2, which reduces the generation of carbon deposition to a large extent on active metals surface and therefore, effectively inhibiting the deactivation of the catalysts.

The surface structures of promoted and unpromoted catalysts were investigated by XPS methods. Fig. 3 displays the Co 2p, Ce 3d and O 1s scans of fresh samples. As shown in Fig. 3a,

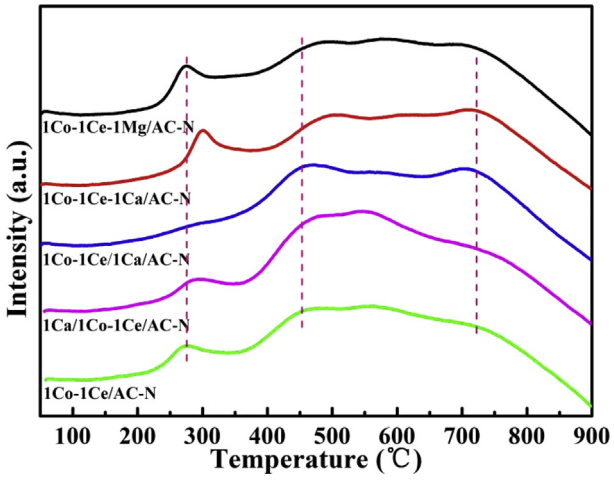

Fig. 1 – H_2-TPR profiles of calcined catalysts1Co-1Ce-1Mg/AC-N, 1Co-1Ce-1Ca/AC-N, 1Co-1Ce/1Ca/AC-N, 1Ca/1Co-1Ce/AC-N and 1Co-1Ce/AC-N.

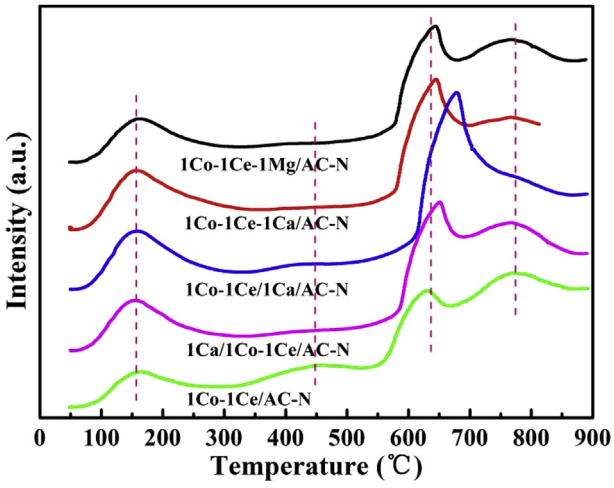

Fig. 2 – CO_2-TPD profile of calcined catalysts 1Co-1Ce-1Mg/AC-N, 1Co-1Ce-1Ca/AC-N, 1Co-1Ce/1Ca/AC-N, 1Ca/1Co-C1e/AC-N and 1Co-1Ce/AC-N.

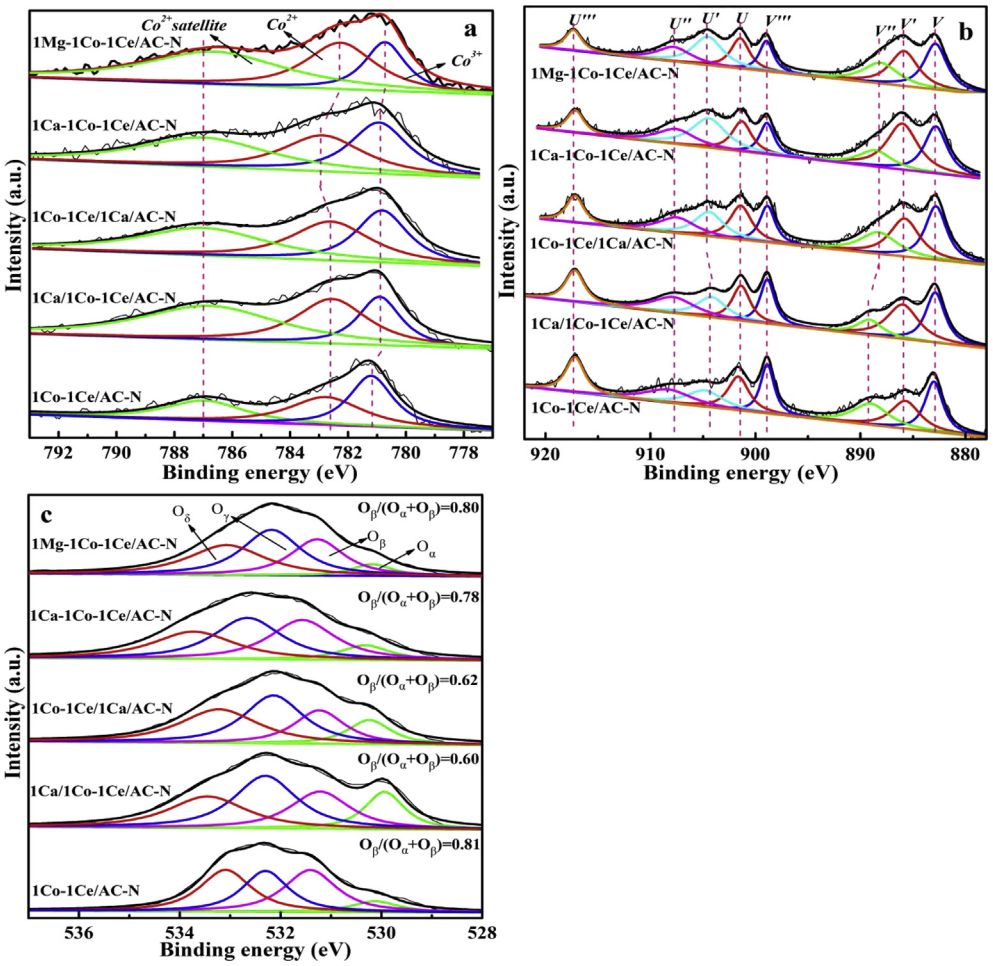

Fig. 3 – (a) Co 2p, (b) Ce 3d and (c) O 1s scan of calcined catalysts 1Co-1Ce-1Mg/AC-N, 1Co-1Ce-1Ca/AC-N, 1Co-1Ce/1Ca/AC-N, 1Ca/1Co-1Ce/AC-N and 1Co-1Ce/AC-N.

XPS spectra Co $2p_{3/2}$ regions could be deconvoluted into three peaks, the peaks around 780.9 and 782.8 eV could be ascribed to the Co^{3+} and Co^{2+}, respectively [61]. A peak at 787.0 eV correspond to the satellite peak. As for 1Co-1Ce-1Ca/AC-N catalyst, based on the peaks area of Co^{3+} and Co^{2+} species, the content of Co^{2+} was basically similar to that of Co^{3+}, Co^{2+}/Co^{3+} ratio is close to 1 (Table 1). The catalyst promoted by Mg exhibited the highest Co^{2+}/Co^{3+} ratio (1.62). The core level spectrum of Ce 3d is presented in Fig. 3b, the complex spectrum comprising of both Ce_2O_3 and CeO_2 are donated with letters U and V to demonstrate the spin-orbit state, the Ce $3d_{3/2}$ and Ce $3d_{5/2}$ spin-orbit state were labeled with U and V, respectively [62]. The characteristic peaks for Ce^{4+} cations are donated as U and V′ and for Ce^{3+} species are donated as U′, U″, U‴, V, V″, V‴. For all promoted catalysts, the addition of promoters improved the content of Ce^{3+}, the 1Co-1Ce-1Ca/AC-N possessed the highest Ce^{3+}/Ce^{4+} ratio (0.5). It is well-known that the increase of Ce^{3+} content could promote the oxygen vacancies generation [62]. In addition, the increasing of content of Ce^{3+} cations expand the opportunities of combination between Ce^{3+} and oxygen vacancies to generate chemisorbed oxygen, the generation of chemisorbed oxygen can further promote the methane oxidation rate. The O1s spectra of promoted and unpromoted catalysts have four different peaks in Fig. 3c. One situated around 530 eV is attributed to the lattice oxygen (O_α), and another peak around 531 eV is ascribed to the adsorbed oxygen (O_β) [63]. The peaks donated as O_δ and O_γ in all catalysts correspond to the oxygen groups (C-OH, C-O-C and O-C=O) [64,65]. For both catalysts promoted with Ca and prepared by sequential impregnation,

Table 1 – XPS derived atomic ratio of different catalysts.

Catalysts	Co (%)	Ce (%)	O (%)	Co^{2+}/Co^{3+}	Ce^{3+}/Ce^{4+}	$O_\beta/(O_\alpha+O_\beta)$
1Co-1Ce-1Mg/AC-N	0.52	0.41	10.47	1.62	0.46	0.80
1Co-1Ce-1Ca/AC-N	0.60	0.41	10.91	0.99	0.50	0.78
1Co-1Ce/1Ca/AC-N	1.47	0.35	11.29	1.15	0.43	0.62
1Ca/1Co-1Ce/AC-N	0.65	1.06	12.71	1.55	0.44	0.60
1Co-1Ce/AC-N	0.83	0.70	17.10	0.91	0.36	0.81

the peak area of O_α increased and the ratio of $O_\beta/(O_\alpha+O_\beta)$ is lower than other catalysts (Table 1), implying the reduction of the level of chemisorbed oxygen. However, higher $O_\beta/(O_\alpha+O_\beta)$ ratio on other catalysts can increase methane oxidation rate and surface chemisorbed oxygen can also promote the electron transfer rate.

The particle size and particle size distribution of different calcined catalysts were performed by TEM analysis. As revealed in Fig. 4, the black dots were associated to Co particles, the Ca promoted catalysts exhibited more homogeneous particle distribution than that of Mg promoted. As shown in Fig. 4b the active metals were homogeneously distributed on the surface of catalyst and the average particle size for 1Co-1Ce-1Ca/AC-N is small and active metal particle size was mainly distributed at 25–30 nm. It is recognized that the carbon deposition of Co-based catalysts is also related to the metallic particle size [66].

The stability analysis was performed at 800 °C for 750 min, the CH_4 and CO_2 conversions are shown in Fig. 5. It is well-known that the side reactions (CH_4=C+2H_2, CO=C+CO_2) can promote the generation of carbon deposition during DRM reaction. As showed in Fig. 5a and b, significant distinction for the conversions of CH_4 and CO_2 can be obviously seen with the increase of time on stream. It can be observed that the 1Co-1Ce-1Ca/AC-N catalyst exhibited higher catalytic performance after the incorporation of Ca to 1Co-1Ce/AC-N. This is consistent with the CO_2-TPD and H_2-TPR analysis results that the addition of Ca led to a significant rise in the catalytic performance which due to stronger basic sites and higher interaction between support and metals. The higher dispersion and smaller particle size of active metals characterized by TEM further confirmed that 1Co-1Ce-1Ca/AC-N displayed optimum catalytic performance. In addition, the sequence of dipping promoter had significant effect on catalytic performance. The CH_4 and CO_2 conversions decreased rapidly then reached to 30% and 53%, respectively, after continuous reaction at 800 °C for 560 min for 1Co-1Ce/1Ca/AC-N. Although the catalytic activity of Mg promoted was lower than unpromoted catalyst, this catalyst exhibited relatively excellent stability. The conversions of CH_4 and CO_2 dramatically decreased and gradually became stable at the beginning of test for all samples. The sharp reduction of catalytic performance of catalysts is speculated to due to the metal dispersion decays rapid [67]. Fig. 5c shows the ratio of H_2/CO varied with reaction time. The H_2/CO ratios of all catalysts is less than 1 and the H_2/CO ratio decreased for all promoted catalysts. Moreover, the CO_2 conversion is higher than CH_4 conversion for all samples, mainly as a result of the occurrence of RWGS reaction (CO_2+H_2=CO+H_2O ΔH_{298K} = 41.1 kJ/mol). The ratio of H_2/CO on 1Co-1Ce/AC-N remains stable at about 0.71 in 12 h and is much higher than that on 1Co-1Ce/1Ca/AC-N in 560 min, which decreased from 0.64 to 0.41. Compared with unpromoted catalyst, the H_2/CO ratio for catalyst, which was promoted with Ca and prepared with co-impregnation slightly decreased.

Fig. 6 displays the XRD patterns of fresh and spent catalysts, it can be seen that all fresh catalysts exhibited

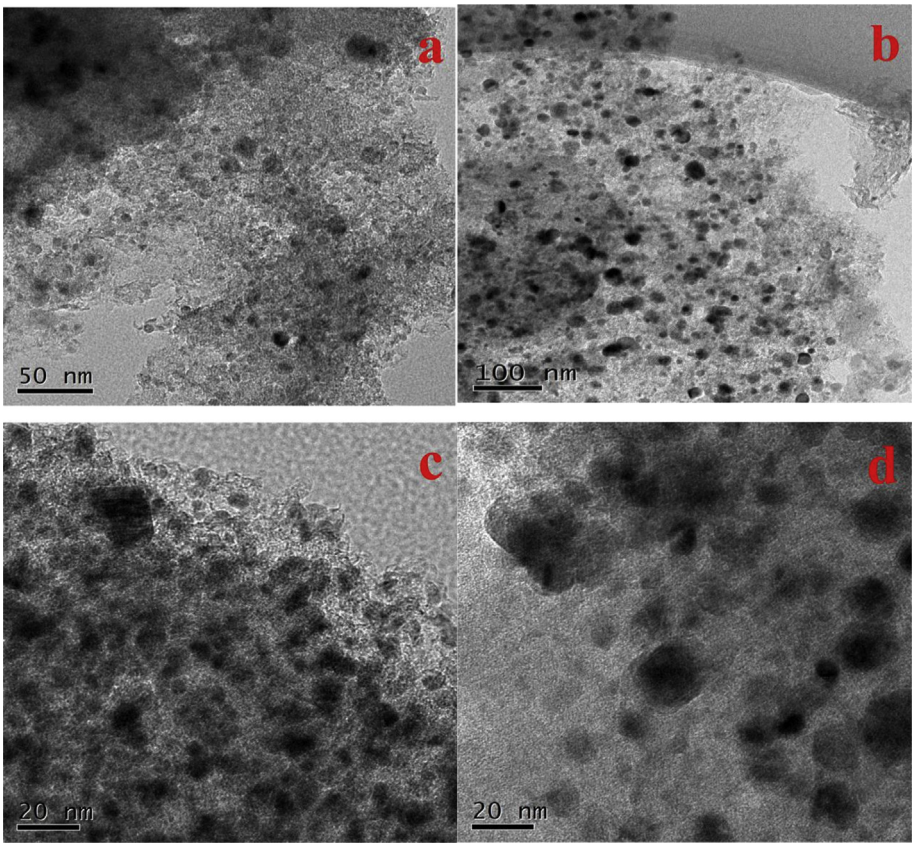

Fig. 4 – TEM images of calcined catalysts (a) 1Co-1Ce-1Mg/AC-N, (b) 1Co-1Ce-1Ca/AC-N, (c) 1Co-1Ce/1Ca/AC-N and (d) 1Ca/1Co-1Ce/AC-N.

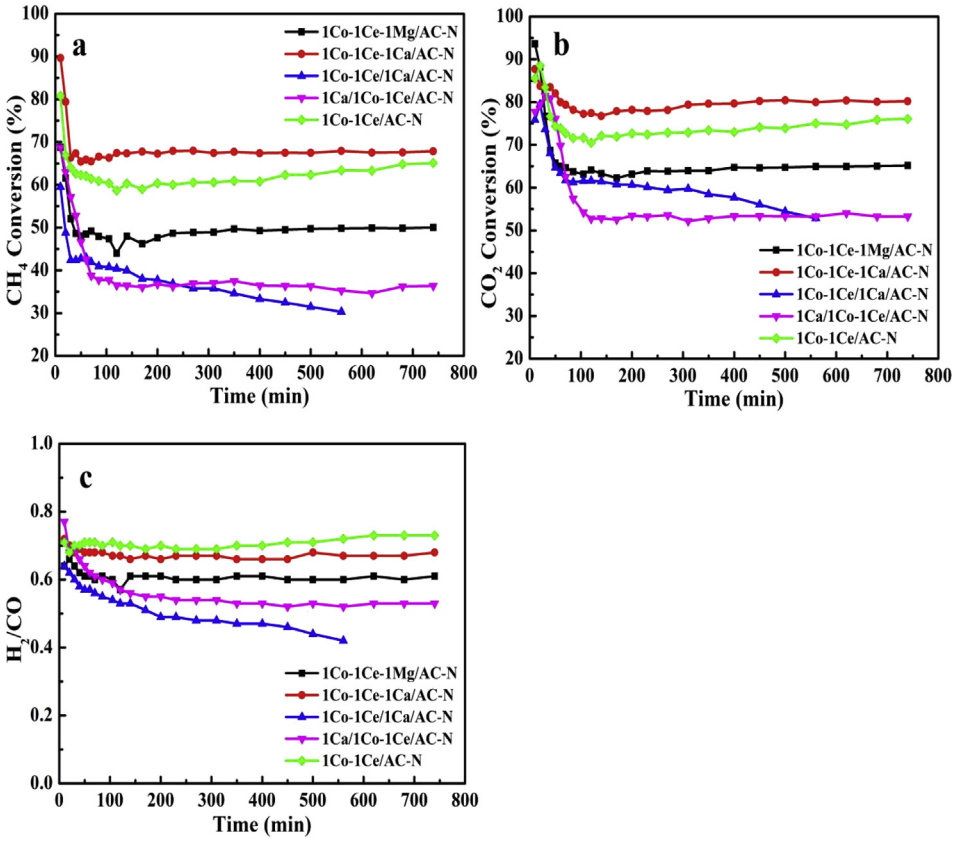

Fig. 5 – CH_4 (a), CO_2 (b) conversion and H_2/CO ratio (c) of calcined catalysts 1Co-1Ce-1Mg/AC-N, 1Co-1Ce-1Ca/AC-N, 1Co-1Ce/1Ca/AC-N, 1Ca/1Co-1Ce/AC-N and 1Co-1Ce/AC-N.

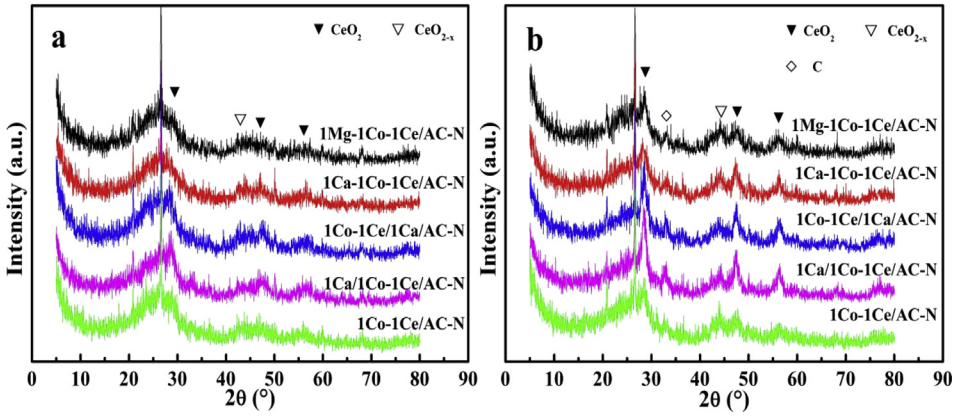

Fig. 6 – XRD patterns of fresh (a) and spent (b) catalysts.

diffraction peaks belonged to CeO_2 (JCPDF no. 43-1002) and CeO_{2-x} (JCPDF no. 49-1415), indicating that the cerium was successfully impregnated on the catalyst. Compared with fresh catalysts, the peak at 28.55°, 43.91°, 47.48° and 56.34° become broader and sharper, which mainly due to that the part of Ce^{3+} was oxidized to Ce^{4+}. For all spend catalysts, the peak at 31.13° attributed to C (JCPDF no. 46-0945) and the intensity of this peak for the catalysts promoted by Ca and prepared by sequential impregnation was much sharper than other spent catalysts, indicating that more carbon deposition was generated on these two catalysts.

The TEM images of samples after long term DRM reaction were carried out for better understand of the carbon deposition and sintering in the process of stability testing. Fig. 7 displays the TEM micrograph of promoted catalysts after 750 min reaction. Obviously, great changes took place for 1Co-1Ce/1Ca/AC-N and 1Ca/1Co-1Ce/AC-N. Fig. 7c clearly displays a large amount of carbon nanotubes on the spent 1Co-1Ce/1Ca/AC-N, which is in accordance with XRD analysis results and further demonstrates poor stability of this catalyst. A large amount of carbon nanotubes was generated might mainly due to the higher concentration of basic sites of the

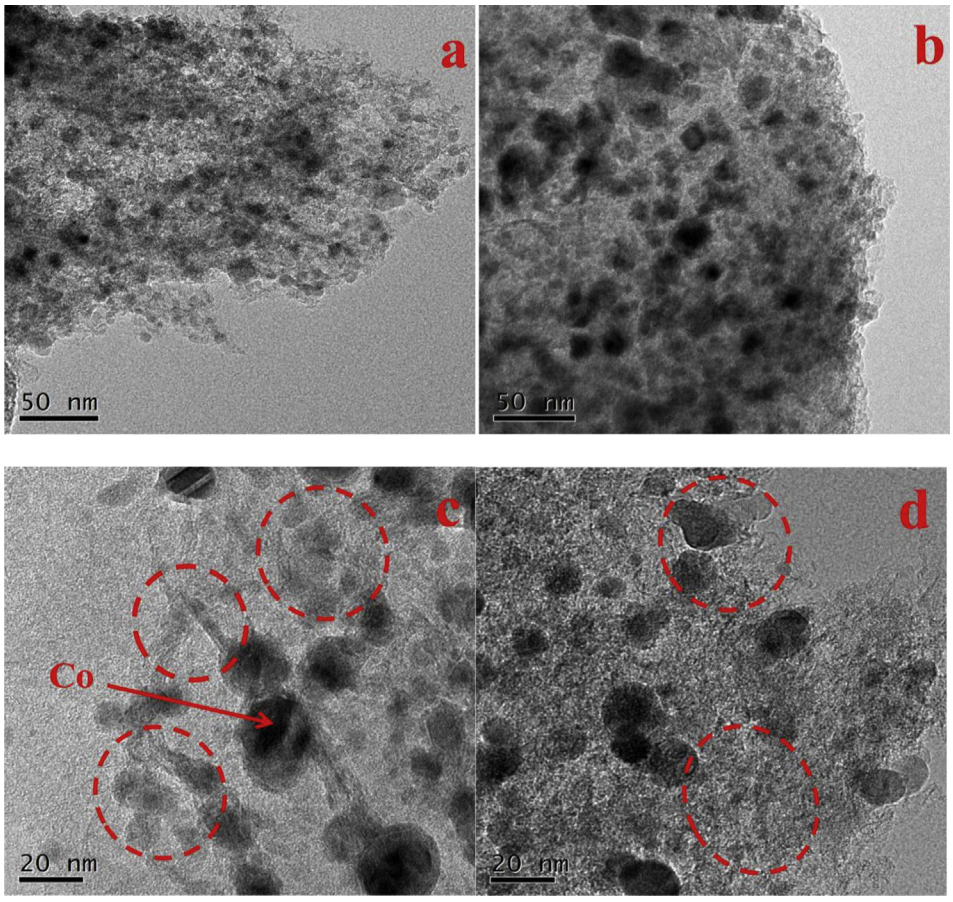

Fig. 7 – TEM images of spent catalysts (a) 1Co-1Ce-1Mg/AC-N, (b) 1Co-1Ce-1Ca/AC-N, (c) 1Co-1Ce/1Ca/AC-N and (d) 1Ca/1Co-1Ce/AC-N.

1Co-1Ce/1Ca/AC-N. Also, a large number of active metal particles were encapsulated by the carbon nanobutes which generated during the process of DRM reaction, causing catalyst deactivation in a relatively short period of reaction time. However, for 1Co-1Ce-1Ca/AC-N, the active metal particles were still well dispersed on support surface, which might be attributed to the synergetic effect that occurred at the interface of metals and carbon support and the particles fixed firmly on the surface of catalyst. The TEM image of spent 1Co-1Ce-1Ca/AC-N is particularly compatible with H_2-TPR analysis result.

Raman spectroscopy was carried out to investigated the degree of graphitization characteristics of the carbon deposition generated on the spent samples. Fig. 8 shows the Raman spectra of spent catalysts, it could be observed that all catalysts showed two peaks in the range between 1000 and 2000 cm^{-1}. The peaks around 1350 and 1596 cm^{-1} can be attributed to the characteristic D and G bands, respectively [68]. The D band is attributed to the defects and disorders of the imperfect structural carbons and the G band is associated with the vibrations of perfect graphite carbon. The peak areas ratio of the D and G (I_D/I_G) bands is used to estimate the graphitic degree and the amount defects in spent catalysts, a low I_D/I_G ratio indicating higher structural perfection of the spent catalysts. The ratio of I_D/I_G was determined to 1Co-1Ce/1Ca/AC-N (1.70) < 1Co-1Ce-1Mg/AC-N (1.72) < 1Co-1Ce-1Ca/AC-N (1.74) < 1Ca/1Co-C1e/AC-N (1.77) < 1Co-1Ce/AC-N (1.78). This demonstrated that the degree of graphitization increased for spent 1Co-1Ce/1Ca/AC-N, which are in consistent with its catalytic performance that CH_4 and CO_2 conversions decreased rapidly with reaction time. Moreover, the Raman analysis results are also in good agreement with TEM results

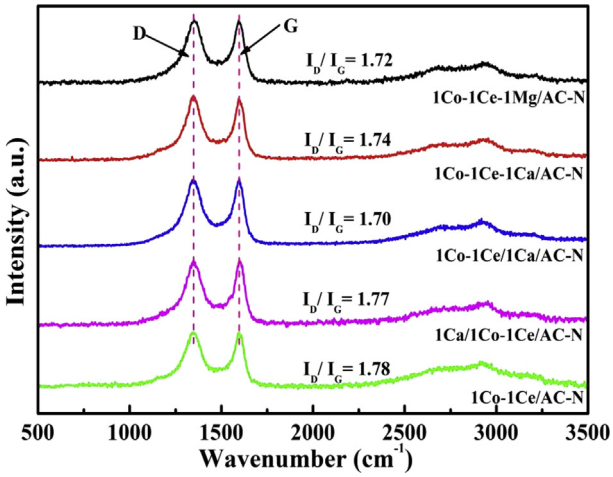

Fig. 8 – Raman spectra of spent catalysts 1Co-1Ce-1Mg/AC-N, 1Co-1Ce-1Ca/AC-N, 1Co-1Ce/1Ca/AC-N, 1Ca/1Co-C1e/AC-N and 1Co-1Ce/AC-N.

that large number of carbon nanotubes were generated on the surface of spent catalyst.

Conclusions

The influence of promoters (Ca and Mg) on catalytic performance of Co-Ce bimetallic catalyst for DRM reaction was studied. The influence of impregnation sequence of the active metals and promoters was also studied. The catalyst promoted with Ca and prepared by co-impregnation exhibited the highest catalytic performance. XPS results indicated the 1Co-1Ce-1Ca/AC-N has the highest amount of Ce^{3+} as well as the same content of Co^{2+} and Co^{3+}. The higher concentration of Ce^{3+} was contributed to the generation of oxygen vacancies, which significantly enhance the oxygen storage capacity and accelerate the adsorption and dissociation of CO_2. Compared with unpromoted catalyst, the basic sites content significantly increased for the promoted catalysts. The impregnation sequence has significant effect on catalytic performance, the samples with different impregnation order of promoter Ca exhibited different catalytic performance and coking resistance ability.

Acknowledgments

This work was supported by the National Natural Science Foundation of China (Nos. 21676174, U1610115 and 21878200), International S&T Cooperation Program of Shanxi province (201703D421038), Shanxi Scholarship Council of China (2017-036), and Joint Fund of Shanxi Provincial Coal Seam Gas (2015012019).

REFERENCES

[1] Cui Y, Liu Q, Yao Z, Dou B, Shi Y, Sun Y. A comparative study of molybdenum phosphide catalyst for partial oxidation and dry reforming of methane. Int J Hydrogen Energy 2019;44:11441–7.
[2] Li D, Li X, Gong J. Catalytic reforming of oxygenates: state of the art and future prospects. Chem Rev 2016;116:11529–653.
[3] Golestan S, Mirzaei AA, Atashi H. Fischer-Tropsch synthesis over an iron–cobalt–manganese (ternary) nanocatalyst prepared by hydrothermal procedure: effects of nanocatalyst composition and operational conditions. Int J Hydrogen Energy 2017;42:9816–30.
[4] Lv S, Liu C, Wang HG, Zhang Y, Wang L. Structural evolution of carbon in Fe@C catalyst during Fischer-Tropsch synthesis reaction. Catal Sci Technol 2019;9:1013–20.
[5] Zhang X, Yang C, Zhang Y, Yan X, Shang S, Yin Y. Ni-Co catalyst derived from layered double hydroxides for dry reforming of methane. Int J Hydrogen Energy 2015;40:16115–26.
[6] Xie H, Yu Q, Zhang Y, Zhang J, Liu J, Qin Q. New process for hydrogen production from raw coke oven gas via sorption-enhanced steam reforming: thermodynamic analysis. Int J Hydrogen Energy 2017;42:2914–23.
[7] Tian H, Li X, Zeng L, Gong J. Recent advances on the design of group VIII base-Metal catalysts with encapsulated structures. ACS Catal 2015;5:4959–77.
[8] Li S, Gong J. Strategies for improving the performance and stability of Ni-based catalysts for reforming reactions. Chem Soc Rev 2014;43:7245–56.
[9] Hou C, Xia G, Xia S, Yu W, Chao J, Yan Z, Li M, Hu Z, Nie H, Li D. Thermodynamics of oxidation of an alumina-supported cobalt catalyst by water in F-T synthesis. Catal Today 2016;264:91–7.
[10] Figen HE, Baykara SZ. Hydrogen production by partial oxidation of methane over Co based, Ni and Ru monolithic catalysts. Int J Hydrogen Energy 2015;40:7439–51.
[11] Li D, Zeng L, Li X, Wang X, Ma H, Assabumrungrat S, Gong J. Ceria-promoted Ni/SBA-15 catalysts for ethanol steam reforming with enhanced activity and resistance to deactivation. Appl Catal B Environ 2015;176–177:532–41.
[12] Wu G, Zhang C, Li S, Han Z, Wang T, Ma X, Gong J. Hydrogen production via glycerol steam reforming over Ni/Al_2O_3: influence of nickel precursors. ACS Sustainable Chem Eng 2013;1:1052–62.
[13] Wang T, Ma H, Zeng L, Li D, Tian H, Xiao S, Gong J. Highly loaded Ni-based catalysts for low temperature ethanol steam reforming. Nanoscale 2016;8:10177–87.
[14] Hu X, Dong D, Shao X, Zhang L, Lu G. Steam reforming of acetic acid over cobalt catalysts: effects of Zr, Mg and K addition. Int J Hydrogen Energy 2017;42:4793–803.
[15] Wu G, Li S, Zhang C, Wang T, Gong J. Glycerol steam reforming over perovskite-derived nickel-based catalysts. Appl Catal B Environ 2014;144:277–85.
[16] Zeng L, Cheng Z, Fan JFL, Gong J. Metal oxide redox chemistry for chemical looping processes. Nature Rev. Chem 2018;2:349–64.
[17] Gao X, Liu G, Wei Q, Yang G, Masaki M, Peng X, Yang R, Tsubaki N. Carbon nanofibers decorated SiC foam monoliths as the support of anti-sintering Ni catalyst for methane dry reforming. Int J Hydrogen Energy 2017;42:16547–56.
[18] Figueira CE, Junior PFM, Giudici R, Alves RMDB, Schmal M. Nanoparticles of Ce, Sr, Co in and out the multi-walled carbon nanotubes applied for dry reforming of methane. Appl Catal A Gen 2017;550:297–307.
[19] Ma Q, Ding W, Wu M, Zhao T, Yoneyama Y, Tsubaki N. Effect of catalytic site position: nickel nanocatalyst selectively loaded inside or outside carbon nanotubes for methane dry reforming. Fuel 2013;108:430–8.
[20] Castro CS, Guerreiro MC, Oliveira LCA, Gonçalves M, Anastácio AS, Nazzarro M. Iron oxide dispersed over activated carbon: support influence on the oxidation of the model molecule methylene blue. Appl Catal A Gen 2009;367:53–8.
[21] Zhao J, Xu J, Xu J, Zhang T, Di X, Ni J, Li X. Enhancement of Au/AC acetylene hydrochlorination catalyst activity and stability via nitrogen-modified activated carbon support. Chem Eng J 2015;262:1152–60.
[22] Jafari A, Saadatjou N, Sahebdelfar S. Influence of chemical treatments of activated carbon support on the performance and deactivation behavior of promoted Ru catalyst inammonia synthesis. Int J Hydrogen Energy 2015;40:3659–71.
[23] Damyanova S, Pawelec B, Arishtirova K, Huerta MVM, Fierro JLG. The effect of CeO_2 on the surface and catalytic properties of Pt/CeO_2-ZrO_2 catalysts for methane dry reforming. Appl Catal B Environ 2009;89:149–59.
[24] Benrabaa R, Barama A, Boukhlouf H, Guerrero-Caballero J, Rubbens A, Bordes-Richard E, Löfberg A, Vannier RN. Physico-chemical properties and syngas production via dry reforming of methane over $NiAl_2O_4$ catalyst. Int J Hydrogen Energy 2017;42:12989–96.
[25] Ma H, Zeng L, Tian H, Li D, Wang X, Li X, Gong J. Efficient hydrogen production from ethanol steam reforming over La-modified ordered mesoporous Ni-based catalysts. Appl Catal B Environ 2016;181:321–31.

[26] Cheng H, Feng S, Wei T, Lu X, Yao W, Li G, Zhou Z. Effects of noble metal-doping on Ni/La_2O_3-ZrO_2 catalysts for dry reforming of coke oven gas. Int J Hydrogen Energy 2014;39:12604–12.
[27] Song H, OZKAN, Umit S. Ethanol steam reforming over Co-based catalysts : role of oxygen mobility. J Catal 2009;261:66–74.
[28] Yu M, Zhu YA, Yong L, Tong G, Zhu K, Zhou X. The promoting role of Ag in Ni-CeO_2 catalyzed CH_4-CO_2 dry reforming reaction. Appl Catal B Environ 2015;165:43–56.
[29] Mousavi SM, Meshkani F, Rezaei M. Preparation of nanocrystalline Zr, La and Mg-promoted 10% Ni/$Ce_{0.95}Mn_{0.05}O_2$ catalysts for syngas production via dry reforming reaction. Int J Hydrogen Energy 2018;43:6532–8.
[30] Fidalgo B, Zubizarreta L, Bermúdez JM, Arenillas A, Menéndez JA. Synthesis of carbon-supported nickel catalysts for the dry reforming of CH_4. Fuel Process Technol 2010;91:765–9.
[31] Kim D, Zussblatt NP, Chung HT, Becwar SM, Zelenay P, Chmelka BF. Highly graphitic mesoporous Fe,N-Doped carbon materials for oxygen reduction electrochemical catalysts. ACS Appl Mater Interfaces 2018;10:25337–49.
[32] Wang K, Ming X, Yan G, Gu Z, Qi HF. Symmetric supercapacitors using urea-modified lignin derived N-doped porous carbon as electrode materials in liquid and solid electrolytes. J Power Sources 2016;332:180–6.
[33] Chang HC, Park SH, Woo SI. Facile growth of N-doped CNTs on Vulcan carbon and the effects of iron content on electrochemical activity for oxygen reduction reaction. Int J Hydrogen Energy 2012;37:4563–70.
[34] Muthukrishnan A, Nabae Y, Okajima T, Ohsaka T. Kinetic approach to investigate the mechanistic pathways of oxygen reduction reaction on Fe-containing N-doped carbon catalysts. ACS Catal 2015;5:5194–202.
[35] Lu HS, Zhang H, Liu R, Xian Z, Zhao H, Wang G. Macroscale cobalt-MOFs derived metallic Co nanoparticles embedded in N-doped porous carbon layers as efficient oxygen electrocatalysts. Appl Surf Sci 2017;392:402–9.
[36] He Q, Mukerjee S, Zeis R, Parres-Esclapez S, Illán-Gómez MJ, Bueno-López A. Enhanced Pt stability in MO_2 (M = Ce, Zr or $Ce_{0.9}Zr_{0.1}$)-promoted Pt/C electrocatalysts for oxygen reduction reaction in PAFCs. Appl Catal A Gen 2010;381:54–65.
[37] Chen S, Zeng L, Tian H, Li X, Gong J. Enhanced lattice oxygen reactivity over Ni-modified WO_3-based redox catalysts for chemical looping partial oxidation of methane. ACS Catal 2017;7:3548–59.
[38] Wang N, Chu W, Zhang T, ZHAO Xiu S. Manganese promoting effects on the Co-Ce-Zr-O_x nano catalysts for methane dry reforming with carbon dioxide to hydrogen and carbon monoxide. Chem Eng J 2011;170:457–63.
[39] Martono E, Vohs JM. Support effects in cobalt-based ethanol steam reforming catalysts: reaction of ethanol on Co/CeO_2/YSZ(100) model catalysts. J Catal 2012;291:79–86.
[40] Do JY, Chava RK, Son N, Kim J, Park NK, Lee D, Seo MW, Ryu HJ, Chi JH, Kang M. Effect of Ce doping of Co/Al_2O_3 catalyst on hydrogen production via propane steam reforming. Catalysts 2018;8(10):413. https://doi.org/10.3390/catal8100413.
[41] Paksoy AI, Caglayan BS, Aksoylu AE. A study on characterization and methane dry reforming performance of Co-Ce/ZrO_2 catalyst. Appl Catal B Environ 2015;168–169:164–74.
[42] Paksoy AI, Caglayan BS, Ozensoy E, Ökte AN, Aksoylu AE. The effects of Co/Ce loading ratio and reaction conditions on CDRM performance of Co Ce/ZrO_2 catalysts. Int J Hydrogen Energy 2018;43:4321–34.
[43] Bertole CJ, Mims CA, Kiss G. Support and rhenium effects on the intrinsic site activity and methane selectivity of cobalt Fischer-Tropsch catalysts. J Catal 2004;221:191–203.
[44] Bezemer GL, Radstake PB, Falke U, Oosterbeek H, Kuipers HPCE, van Dillen AJ, de Jong KP. Investigation of promoter effects of manganese oxide on carbon nanofiber-supported cobalt catalysts for Fischer-Tropsch synthesis. J Catal 2006;237:152–61.
[45] Osakoo N, Henkel R, Loiha S, Roessner F, Wittayakun J. Effect of support morphology and Pd promoter on Co/SBA-15 for Fischer-Tropsch Synthesis. Catal Commun 2014;56:168–73.
[46] Martinelli M, Mehrbod M, Dawson C, Davis BH, Lietti L, Cronauer DC, Kropf AJ, Marshall CL, Jacobs G. Fischer-Tropsch synthesis: foregoing calcination and utilizing reduction promoters leads to improved conversion and selectivity with Co/silica. Appl Catal A Gen 2018;559:153–66.
[47] Foo SY, Cheng CK, Nguyen TH, Adesina AA. Evaluation of lanthanide-group promoters on Co-Ni/Al_2O_3 catalysts for CH_4 dry reforming. J Mol Catal A Chem 2011;344:28–36.
[48] Alipour Z, Rezaei M, Meshkani F. Effect of alkaline earth promoters (MgO, CaO, and BaO) on the activity and coke formation of Ni catalysts supported on nanocrystalline Al_2O_3 in dry reforming of methane. J Ind Eng Chem 2014;20:2858–63.
[49] Li Z, Wang X, Chen C, Zou X, Lu X. Investigation of mesoporous $NiAl_2O_4$/MOx (M = La, Ce, Ca, Mg)-γ-Al_2O_3 nanocomposites for dry reforming of methane. RSC Adv 2017;7:33143–54.
[50] Kalai DY, Stangeland K, Jin Y, Yu Z. Active and stable hydrotalcite derived Ni catalysts for CO_2 reforming of methane: comparison with catalysts by incipient wetness. J CO_2 Util 2018;25:346–3455.
[51] Németh M, Srankó D, Károlyi J, Somodi F, Schay Z, Sáfrán G, Sajóc I, Horváth A. Na-promoted Ni/ZrO_2 dry reforming catalyst with high efficiency: details of Na_2O-ZrO_2-Ni interaction controlling activity and coke formation. Catal Sci Technol 2017;7:5386–401.
[52] José-Alonso DS, Illán-Gómez MJ, Román-Martínez MC. K and Sr promoted Co alumina supported catalysts for the CO_2 reforming of methane. Catal Today 2011;176:187–90.
[53] Chen Q, Zhang J, Pan B, Kong W, Chen Y, Zhang W, Sun Y. Temperature-dependent anti-coking behaviors of highly stable Ni-CaO-ZrO_2 nanocomposite catalysts for CO_2 reforming of methane. Chem Eng J 2017;320:63–73.
[54] Sengupta S, Deo G. Modifying alumina with CaO or MgO in supported Ni and Ni-Co catalysts and its effect on dry reforming of CH_4. J CO_2 Util 2015;10:67–77.
[55] Casanovas A, Roig M, Leitenburg CD, Trovarelli A, Llorca J. Ethanol steam reforming and water gas shift over Co/ZnO catalytic honeycombs doped with Fe, Ni, Cu, Cr and Na. Int J Hydrogen Energy 2010;35:7690–8.
[56] Jang WJ, Jeong DW, Shim JO, Kim HM, Han WB, Bae JW, Roh HS. Metal oxide (MgO, CaO, and La_2O_3) promoted Ni-$Ce_{0.8}Zr_{0.2}O_2$ catalysts for H_2 and CO production from two major greenhouse gases. Renew Energy 2014;79:91–5.
[57] Cavallaro S, Mondello N, Freni S. Hydrogen produced from ethanol for internal reforming molten carbonate fuel cell. J Power Sources 2001;102:198–204.
[58] Bao T, Zhao Z, Dai Y, Lin X, Jin R, Wang G, Muhammad T. Supported Co_3O_4-CeO_2 catalysts on modified activated carbon for CO preferential oxidation in H_2-rich gases. Appl Catal B Environ 2012;119:62–73.
[59] Karimi A, Nasemejad B, Rashidi AM. Synthesis and characterization of multiwall carbon nanotubes/alumina nanohybrid-supported cobalt catalyst in Fischer-Tropsch synthesis. J Energy Chem 2013;22:582–90.
[60] Kumar P, Srivastava VC, Mishra IM. Dimethyl carbonate synthesis by transesterification of propylene carbonate with

methanol: comparative assessment of Ce-M (M=Co, Fe, Cu and Zn) catalysts. Renew Energy 2016;88:457–64.
[61] Horlyck J, Lawrey C, Lovell EC, Amal R, Scott J. Elucidating the impact of Ni and Co loading on the selectivity of bimetallic NiCo catalysts for dry reforming of methane. Chem Eng J 2018;352:572–80.
[62] Feng XY, Guo JX, Wen XR, Xu MY, Chu YH, Yuan SD. Enhancing performance of Co/CeO_2 catalyst by Sr doping for catalytic combustion of toluene. Appl Surf Sci 2018;445:145–53.
[63] Zhong L, Cai W, Yu Y, Zhong Q. Insights into synergistic effect of chromium oxides and ceria supported on Ti-PILC for NO oxidation and their surface species study. Appl Surf Sci 2015;325:52–63.
[64] Guedidi H, Reinert L, Lévêque JM, Soneda Y, Bellakhal N, Duclaux L. The effects of the surface oxidation of activated carbon, the solution pH and the temperature on adsorption of ibuprofen. Carbon 2013;54:432–43.
[65] Bradley RH, Smith MW, Andreu A, Falco M. Surface studies of novel hydrophobic active carbons. Appl Surf Sci 2011;257:2912–9.
[66] Barroso MN, Gomez MF, Arrúa LA, Abello MC. CoZnAl catalysts for ethanol steam reforming reaction. Chem Eng J 2010;158:225–32.
[67] Djinović P, Črnivec IGO, Pintar A. Biogas to syngas conversion without carbonaceous deposits via the dry reforming reaction using transition metal catalysts. Catal Today 2015;253:155–62.
[68] Chen X, Oh WD, Hu ZT, Sun YM, Webster RD, Li SZ, Lim TT. Enhancing sulfacetamide degradation by peroxymonosulfate activation with N-doped graphene produced through delicately-controlled nitrogen functionalization via tweaking thermal annealing processes. Appl Catal B Environ 2018;225:243–57.